Numerical simulation of transversely impacted, clamped circular aluminium plates

R. Villavicencio, L. Sutherland and C. Guedes Soares

Abstract

This paper presents experimental and numerical results of a series of drop weight impact tests examining the dynamic response of fully clamped aluminium 5083/H111 circular plates struck laterally at the centre by a mass with a spherical indenter. The impact velocity varied from 1.0 to 6.0 m/s. The plates showed no visible damage at the very low incident energies but suffered both indentation and global deformation as incident energy was increased. The numerical modelling was performed using the LS-DYNA non-linear, dynamic finite element software. Both shell and solid element models of progressively refined mesh sizes were used and the results compared with the experimental data. The numerical calculations used can accurately predict the response of deflections, forces and absorbed energies, even for the models with coarse meshes. However, finer meshes and solid elements were required to obtain a satisfactorily accurate prediction of the deformed shape.

Keywords: impact, aluminium, circular plates, numerical simulations, local indentation

1. Introduction

Increased attention is being paid to the assessment of the collision strength of ship structures and to developing more crashworthy designs. One approach to the problem is to use complex finite element (FE) models to calculate the energy absorbed during collision (Akita et al. 1972; Kajaste-Rudnitski et al. 2005). Another approach is to use simple models of energy absorption for each structural member and to calculate the absorbed energy as the collision progresses and the structural elements are subjected to large deformations (McDermott et al. 1974; Amdahl et al. 1995; Wang et al. 1997). The simplified models used to calculate energy absorption are based on rigid plastic theory, and these have been shown to be appropriate for such predictions as described in Guedes Soares (1981), Jones (1989), Stronge and Yu (1993) and Yu and Chen (2000), among others.

Structural design for ship collision requires an accurate prediction of the damage of stiffened plates under impact loading. The FE analysis is a useful tool to predict the extent of ship collision and damage to structural components. However, the non-linear dynamic analysis should be compared with experimental tests before being used for structural design. Unfortunately, experimental tests on full-scale ship collision are extremely expensive and thus very rare. One approach is to perform scaled collision test on typical ship structural members to validate the numerical methods for impact analysis. In a collision between two ships, the side plates suffer the most severe consequences, undergoing permanent deformations across areas wider than the frame spacing. Thus, previous to performing a numerical analysis of the entire ship structure, it is necessary to verify numerical models of

the dynamic large deformation of plates, before then increasing the complexity of the FE model.

Concerning the behaviour of plates, a theoretical analysis that examines the dynamic plastic response of thin circular plates transversely and centrally struck by a mass with a conical head and a spherical nose has been summarized by Shen (1995). The analysis employs an interaction yield surface, which combines the bending moment and membrane forces required for plastic flow. Approximate formulas for the load-deflection relationship of a rigid-plastic circular plate deflected by a rigid sphere were derived by Wang et al. (1998), which studied the behaviour at large deflection, neglecting the contribution from bending moments. Mechanics of the lateral indentation of a rigid sphere into a thin, ductile metal plate were studied by Simonsen and Lauridsen (2000) including experiments, analytical theories and FE calculations. The focus was the prediction of plate failure and the energy absorption until this point. Analytical theories were derived for the load-displacement behaviour of a plastic membrane up to failure. Experimental tests that examined the dynamic response and petalling failure of thin circular plates struck transversely by masses with conical heads were conducted by Shen et al. (2002), where a theoretical analysis of the petalling failure was proposed (Shen 2002).

The purpose of the present work is to compare the results of a series of experimental tests previously reported by Sutherland and Guedes Soares (2009) with a FE analysis using different element types and mesh sizes. The force-displacement curves of the different simulations are compared with the experimental results, and the best approximations are selected for further calculations. The shape of the deformation is analysed considering local indentation and global deflections.

2. Experimental details and summary of results

The experimental tests represent an impact event in which a fully clamped circular plate is struck by a mass *G* travelling with an initial velocity V_0 at the centre of the plate (Figure 1). After impact, the striker *G* is assumed to remain in contact with the plate. Therefore, the striker and the struck point of the plate have an initial velocity V_0 at the instant of contact and a common velocity throughout the entire response. The maximum total deformation W_t is divided into two parts, maximum local indentation W_i and maximum global deflection W (Shen 1995).

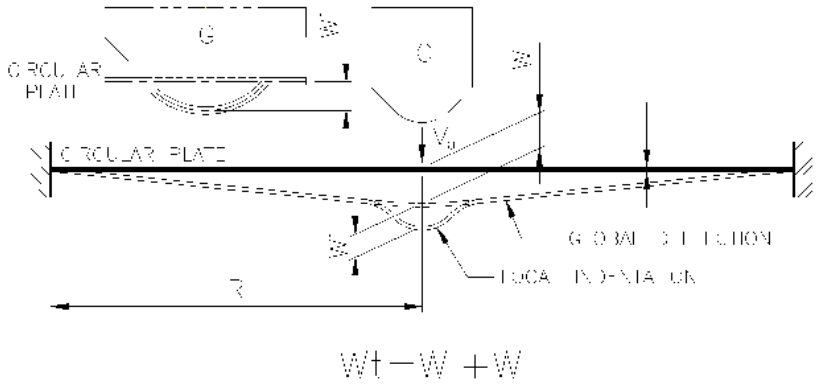

Figure 1 Clamped circular plate struck laterally at the centre by a mass.

Impact testing was performed using a fully instrumented Rosand IFW5 falling weight machine. A small, light hemispherically ended cylindrical projectile was dropped from a known, variable height between guide rails onto clamped horizontally supported circular aluminium 5083/H111 plate targets. A much larger, variable mass was attached to the projectile, and a load cell between the two gave the variation of impact force with time. An optical gate gave the incident velocity of the impact head, and hence the velocity, displacement and the energy it imparted could be calculated from the measured force–time data by successive numerical integrations, knowing the impact mass.

The experimental setup can be seen in Figure 2. Specimen plates were 200 mm square and were fully clamped by four bolts between two thick 200 mm square steel plates with internal diameter *D*= 100 mm. The indenter was a hemispherically ended projectile of radius *r*= 5 mm. In order to investigate the effects of both global deformation and local indentation, tests were carried out for two-plate thickness, 2.0 mm and 5.92 mm, (henceforth referred to as 'thin' and 'thick', respectively) using an impact mass of 3.103 kg and 4.853 kg, respectively. Experimental tests were carried out, in each case on an untested specimen, for a range of impact velocities from very low energies up to perforation, where possible. Full experimental details and discussions of the experimental results may be found in Sutherland and Guedes Soares (2009).

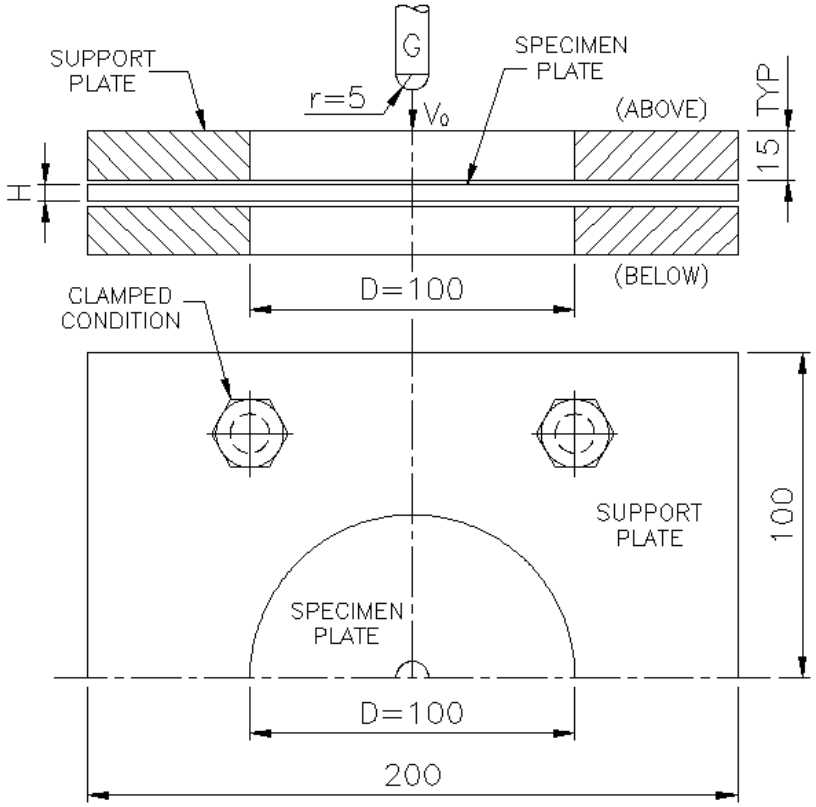

Figure 2 Circular plate specimen in clamped condition (dimensions in millimetres).

A representative sample of the full experimental results at low, medium and high incident energy for both thin and thick plates was selected for comparison with the current numerical analyses, as summarised in Table 1. The 'End' of the test is defined as when the contact force drops to zero and occurs when the indenter first leaves the surface of the plate. Specimens suffering perforation were not considered here.

Specimen	Impact Velocity (m/s)	Values at Peak Force			Values at End	
		Force (kN)	Defln (mm)	Energy (J)	Defln (mm)	Energy (J)
AL1-K	0.95	1.2	2.50	1.6	1.27	1.1
AL1-N	2.53	3.7	5.36	10.6	4.07	9.1
AL1-R	4.39	6.7	9.99	31.2	8.98	29.8
AL1-U	5.90	8.9	12.78	55.7	12.00	55.1
AL2-H	0.91	4.8	0.79	2.3	0.23	1.1
AL2-I	2.62	11.4	2.41	16.8	1.23	12.2
AL2-B	4.77	15.8	5.30	56.8	4.19	52.2
AL2-D	5.85	18.4	6.74	84.0	5.79	80.2

Table 1 Summary of experimental impact results.

3. Numerical model

The computations were carried out using the LS-DYNA (version 971, Hallquist 2005) FE package, which is appropriate for non-linear explicit dynamic simulations with large deformations. The FE model was designed with the following components (Figures 3 and 4): a specimen plate, two support plates (one below and the other above the specimen plate) and the striking mass. The specimen plates were modelled with either shell or solid elements, the support plates with shell elements and the striking mass with solid elements. The shell elements were four-node with five-integration points through the thickness (Belytschko-Lin-Tsay formulation), and the solid elements were eight-node with one-integration point (constant stress solid element formulation); both element formulations are the default in LS-DYNA.

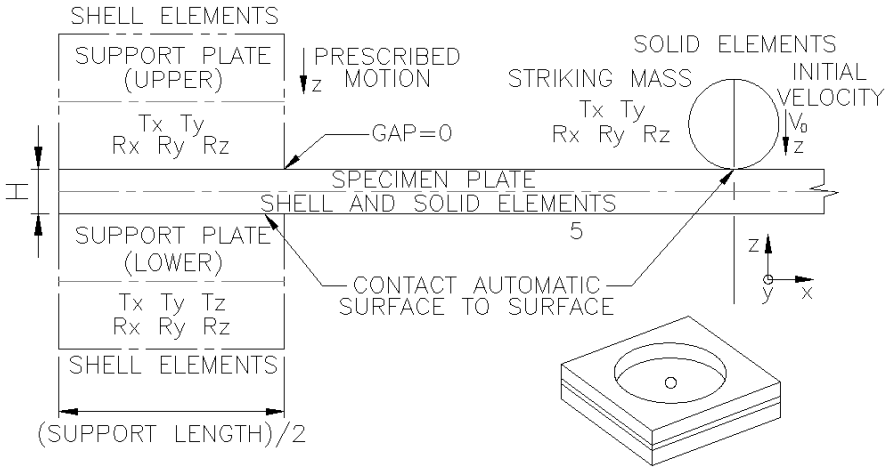

Figure 3 Details of FE model.

3.1. Mesh design

The type of element (shell or solid) and the mesh size used to model the specimen plates were varied in order to optimise the agreement of the FE model with the experimental results. The meshing used in all cases was regular and square (Figure 4), meaning that the mesh was not finer neither at the point of impact nor at the supported perimeter. Initial calculations explored the use of different mesh configurations, some of them automatically generated and others with coincident nodes in the supports and radial orientation of the elements. Similar results were obtained in terms of force-displacement response in all cases, and hence the simplest and cheapest mesh design was selected for all future calculations.

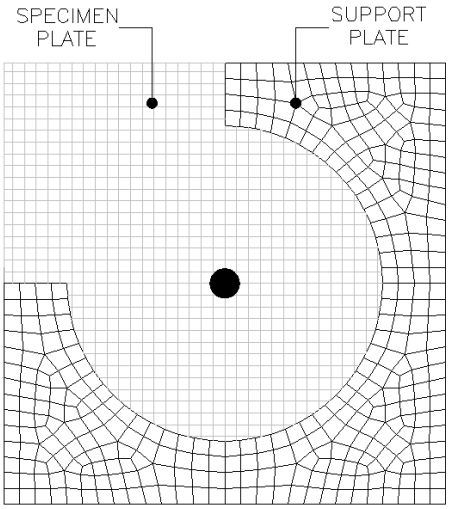

Figure 4 Typical mesh.

The approach taken was to start with a mesh size equal to the plate thickness and then progressively decrease the mesh size until good correlation with the experimental maximum force and displacement results was achieved. It was also important to obtain a good approximation of the shape of the plate deformation, in terms of both local indentation and global deflection.

The mesh size of the shell element models considered were 6 × 6, 4 × 4 and 2 × 2 mm for the thick plates (denoted by Shell6, Shell4 and Shell2, respectively) and 2 × 2, 1 × 1 and 0.5 × 0.5 mm for the thin plates (denoted by Shell2, Shell1 and Shell0.5, respectively). Care was taken to avoid an excessively high element side length to thickness ratio. The solid element model mesh sizes were 1 × 1 × 1 mm for the thin plates (Solid1) and 2 × 2 × 2 and 1 × 1 × 1 mm for the thick plates (Solid2 and Solid1, respectively).

The FE representation of the support plates was used to simulate the experimental clamped boundary condition of the specimen plates using a relatively coarse mesh of shell elements with a side length of approximately 5 mm. The striking mass was modelled using solid elements to avoid initial penetrations on the surface of the specimen plates (for both shell and solid models). It should be mentioned that the striking mass could also have been modelled using shell elements and defining adequately the offset of the projected contact surface. However, in this case the solid indenter simplified the geometry and the indenter-specimen offsets in the FE model. In order to model the spherical geometry sufficiently and accurately, a mesh size of approximately 1.0 mm was chosen. The sphere was meshed to ensure that the face of a sphere element contacted with the plate, ensuring a more realistic

simulation of the contact area as observed in the experiments. Also, it was found in the FE model that when a single-node corner of the sphere contacts first a node of the specimen plate, the force and absorbed energy time data experienced unrealistic peaks at the beginning of the response.

The radius of the impacting mass is 5.0 mm, and hence the ratios of element size to indenter radius were 6/5, 4/5, 2/5, 1/5 and 1/10 for meshes with element side length 6, 5, 4, 2, 1 and 0.5 mm, respectively. These ratios play an important role when the shape of the deformation is analysed.

3.2. Boundary conditions

In the present FE model, the support plates simulate the boundary conditions of the specimen plate, compressing the specimen as occurred in the experiments (Figure 3). Only half of the support plate length compressing the specimen was modelled since this reduced the computational cost while previous numerical analyses showed that this did not affect the results. No gap between the support plates and the specimen plate was modelled.

The lower support plate was constrained in all degrees of freedom (Figure 3). The upper support plate was constrained in all degrees of freedom except for vertical translation, because a prescribed vertical motion was imposed to compress the specimen plate to simulate the clamped condition. The value of the prescribed displacement was equal to $\epsilon_y H/3$ (Ehlers 2010), where ϵ_y is the yield strain of the material and H is the thickness of the specimen. For the striking mass, only the vertical translation was free, in which direction the initial impact velocity V_0 was assigned.

3.3. Contact definition

The contact between the striking mass and the specimen plate and between the support plates and the specimen plate were defined as ‘Automatic Surface to Surface’ (Hallquist 2005). A static coefficient of friction of 0.3 in both cases was used and a dynamic coefficient of friction of 0.1 was included in the contact between the striking mass and specimen plate (Ehlers et al. 2007; Ehlers 2010). It should be mentioned that the static coefficient of friction differs from the value proposed in Table 26.1 of Hallquist (2005). However, the defined coefficient in the FE model has been used for steel–steel contact giving good agreement with experimental results. In the present paper the defined value is considered as a first approximation; further analyses would be beneficial to refine the model in terms of this coefficient, especially because it has been found that at high velocity the coefficient of friction decreases.

3.4. Material

Both the support plates were modelled as a rigid material to ensure no deformation. The ‘Mat.020-Rigid’ was selected from the material library of LS-DYNA, assigning mild steel mechanical properties (Young’s modulus 210 GPa and Poisson’s ratio 0.3) and a mass density of 7850 kg.

The striking mass was modelled using the same rigid undeformable material and mechanical properties as the support plates. However, since the falling weight assembly was modelled

as a simple sphere, an artificially large density was used to give the same mass as used in the experiments. The mass densities were 6.5×10^6 and 10.0×10^6 kg/m^3 for the striking mass of 3.103 and 4.853 kg, respectively (a factor of 1.035 was included to allow for the small volume error since the sphere was modelled with a finite number of discrete flat elements).

The definition of the specimen plate material is most important, and thus the mechanical properties of the material used in the FE models were obtained from in-house tensile tests carried out on material cut from the same panels from which the impact specimens were taken, and are summarized in Table 2. The material selected from the library of LS-DYNA was 'Mat.024-Piecewice linear plasticity', which allows the definition of a true stress–strain curve as an offset table.

Property	**Units**	**Aluminium 2.0 mm**	**Aluminium 6.0 mm**
Mass density	kg/m^3	2710	2710
Young's modulus	GPa	65	65
Poisson's ratio	-	0.33	0.33
Yield stress	MPa	125	145
Rupture stress	MPa	285	290

Table 2 Mechanical properties of aluminium 5083/H111.

Since the engineering stress–strain curve does not give a true indication of the deformation characteristics of a metal, it is necessary to use the true stress–strain curve that represents the basic plastic-flow characteristics of the material. The true stress must be based on the actual cross-sectional area of the specimen, but the true strain measurement is measured directly when, as is the case here, strain gauges are used (Dieter 1986).

In the true stress–strain curve until the onset of necking (for most materials, necking begins at maximum load at a value of strain where the true stress equals the slope of the flow curve), the true stress σ_t and the true strain ϵ_t are expressed in terms of engineering stress σ_e and engineering strain ϵ_e by:

$$\sigma_t = \sigma_e(\varepsilon_e + 1) \quad (1)$$

$$\varepsilon_t = \ln(\varepsilon_e + 1) \quad (2)$$

The tensile tests of these particular aluminium plates showed that the true stress at maximum load is almost coincident with the true fracture stress and that very little necking occurred. Hence, the exact true stress–strain curve can be used as input to the numerical models. The true and engineering stress–strain curves for each thickness are shown in Figures 5 and 6. Since only plastic deformation was observed for the experimental impact tests considered here, failure strain was not required to define the material of the specimen plates.

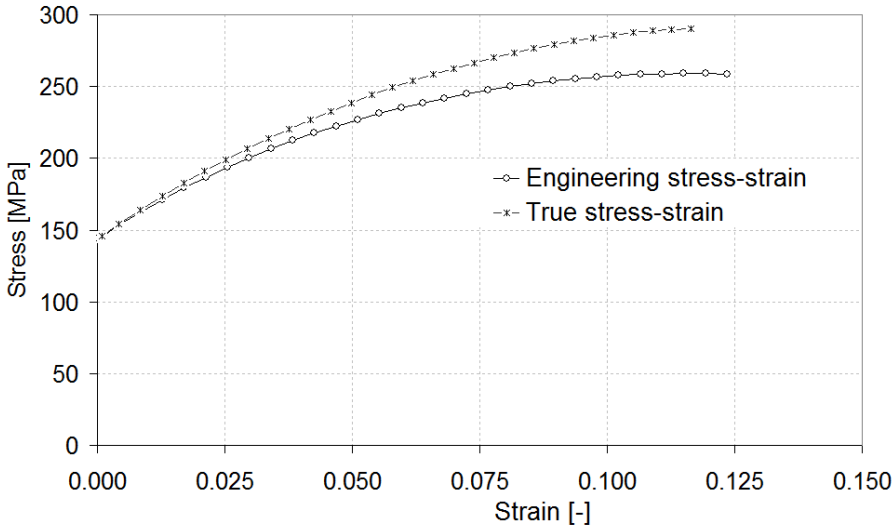

Figure 5 Engineering and true stress–stain curves (experimental). Thickness 5.92 mm.

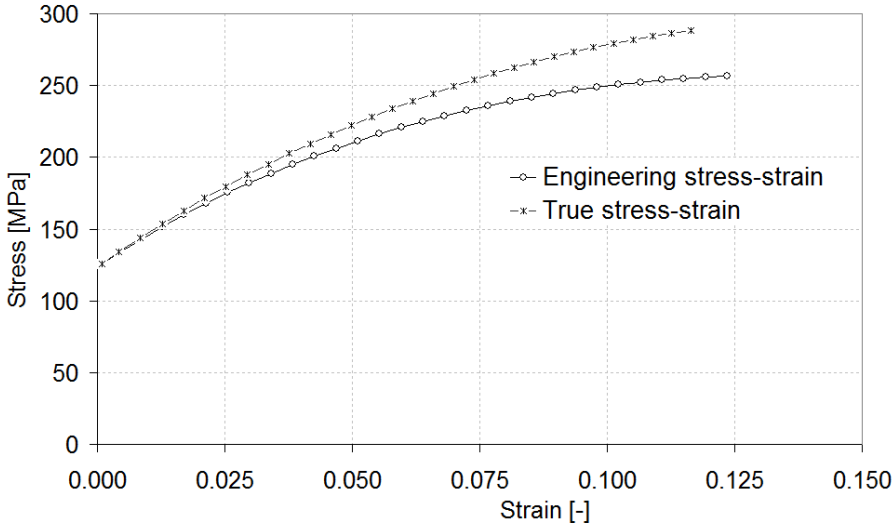

Figure 6 Engineering and true stress–stain curves (experimental). Thickness 2.00 mm.

Published experimental results for aluminium alloy beams (Liu and Jones 1987; Jones 1989) showed that they are essentially strain-rate insensitive, and for the circular plates considered here, the inclusion of nominal strain-rate coefficients in the numerical simulations resulted in smaller displacements than seen in the experimental results. Hence, strain-rate sensitivity was not included in further numerical simulations here. It is important to note that for other materials, such as mild steel, the strain-rate sensitivity should be included (Liu and Jones 1987).

3.5. Tensile test simulation

As was mentioned in Section 3.4, since only plastic deformation was observed for the experimental impact tests considered here, failure was not required to define the material of the specimen plates. However, the experimental tensile tests used to obtain the material mechanical properties were modelled using LS-DYNA, both in order to verify that the impact model gave the correct plastic deformation and also to make an initial attempt at failure

prediction. For a purely plastic response without necking or fracture, the plastic parameters of the material can be determined from the results of a tensile test. However, fracture and necking occur over a length that is much smaller than the side length of the elements considered here, and thus the elements used in the FE model cannot capture such a local phenomenon. Therefore, to model failure, LS-DYNA deletes elements when their average strain reaches a 'critical' value.

Ehlers and Varsta (2009) obtained experimentally true stress–strain material curves from tensile test specimens using highly accurate optical measuring systems. This true material information experimentally determined the failure strain at a small scale, and was used to numerically simulate plate punching experiments obtaining good agreement (Ehlers 2010). However, in the current analysis the material property information is reduced to the engineering stress–strain curve. From this point of view, the mesh sensitivity can be approached with an engineering method at the level of advanced industry practice (Simonsen and Lauridsen 2000) in which the 'critical' failure strain (in this case the average normal strain over the element) required to give the actual experimental material fracture strain is found through numerical simulations of the tensile tests using different failure strains and mesh densities. Here 'failure strain' denotes the strain value when fracture occurs.

In the numerical simulations, only the length of the tensile test specimens between the clamping edges was modelled (Figure 7) and the same mesh sizes used in the circular specimen plates (Shell elements) were considered. The translational degrees of freedom were restricted at one end and a constant displacement of 100 times the experimental speed was prescribed (Ehlers and Varsta 2009) at the other. Default hourglass control was included. The true stress–strain curve used to define the material was the same as that used for the circular plate specimens (Figures 5 and 6). The material model for the tensile tests does not use a specific failure criteria in the purest sense, but the numerical simulation was 'calibrated' using the experimental data to give the 'critical' strain value (averaged over the element) that fit the experimental results by using a trial and error approach. For the tests carried out here, it was not difficult to estimate the first value of failure strain to be used since very little necking was observed in the experiments, and thus the failure strain was close to the axial strain at the initiation of necking. The force of the displaced nodes at the free end is obtained and then plotted versus the applied displacement, and these values used to give the engineering stress–strain behaviour.

The results for different mesh sizes are presented in Figures 8 and 9 for thick and thin plates, respectively. The 'critical' failure strain (used as input in the numerical model) represented in both graphs is 0.15. The dependence of the failure strain on the element size is evident from Figures 8 and 9 (a coarse mesh requires a lower value of failure strain), showing that this parameter is not a true material property in this case. Most numerical simulations of tensile tests in the literature follow the engineering curve quite precisely until the point of necking independently of mesh size (even with relatively coarse meshes), but the post-necking behaviour is usually highly dependent on the mesh size (Simonsen and Lauridsen 2000; Tabri et al. 2007). For the aluminium 5083/H111 tensile tests carried out here, the stress at maximum load was almost coincident with the fracture stress, and very little necking was observed (Figures 5 and 6). Hence, such post-necking modelling problems were avoided, and the plastic response could be equally well modelled using different mesh sizes.

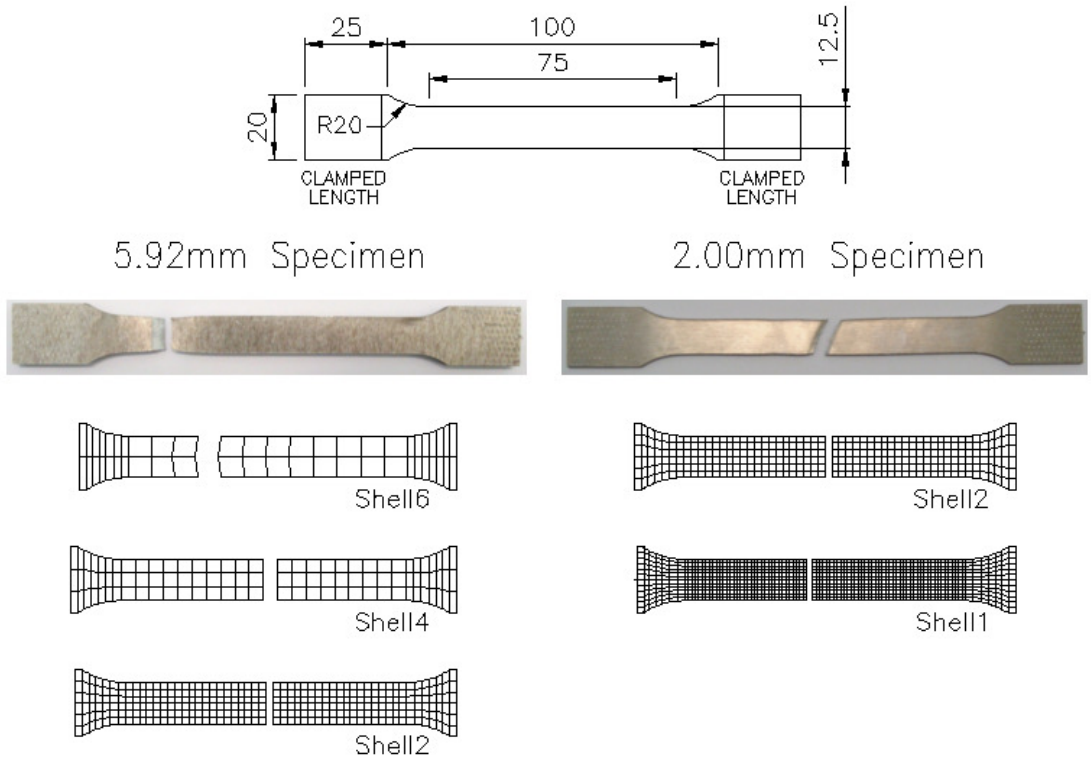

Figure 7 Tensile test specimens and their numerical simulation.

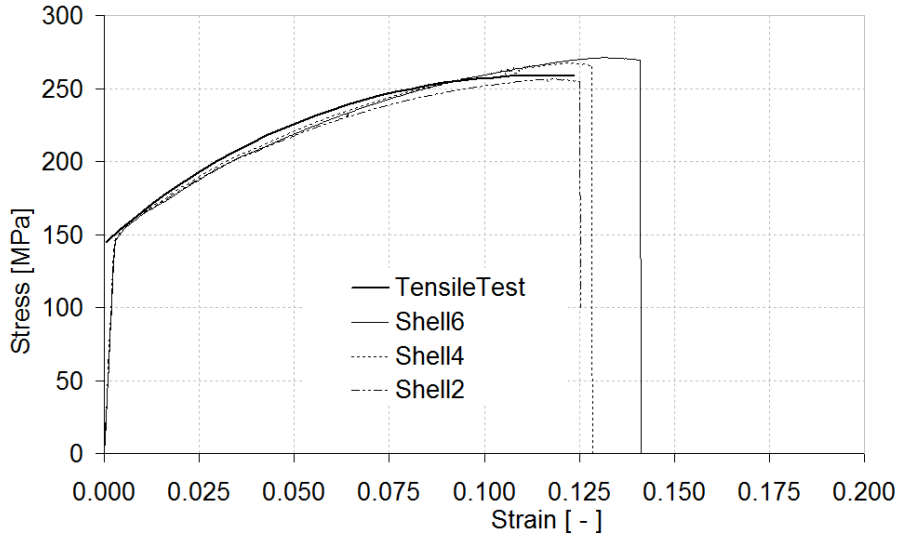

Figure 8 Numerical and experimental engineering stress–strain curves. Thickness 5.92 mm.

For the thick tensile test simulation, Figure 8 shows that all mesh sizes considered predicted the plastic behaviour of the material well. The fact that the Shell4 and Shell6 models overestimate the specimen failure strain shows that a lower value of the material failure strain would be required for the coarser mesh sizes. For the thin specimens, the numerical simulation (Figure 9) for both mesh sizes considered gives almost identical results, both giving approximately 8.0% lower stress values than the experimental results. Again, it is

indicated that for the coarser mesh Shell2 model, a lower value for the material failure strain should be obtained to give a better comparison with the experimental results.

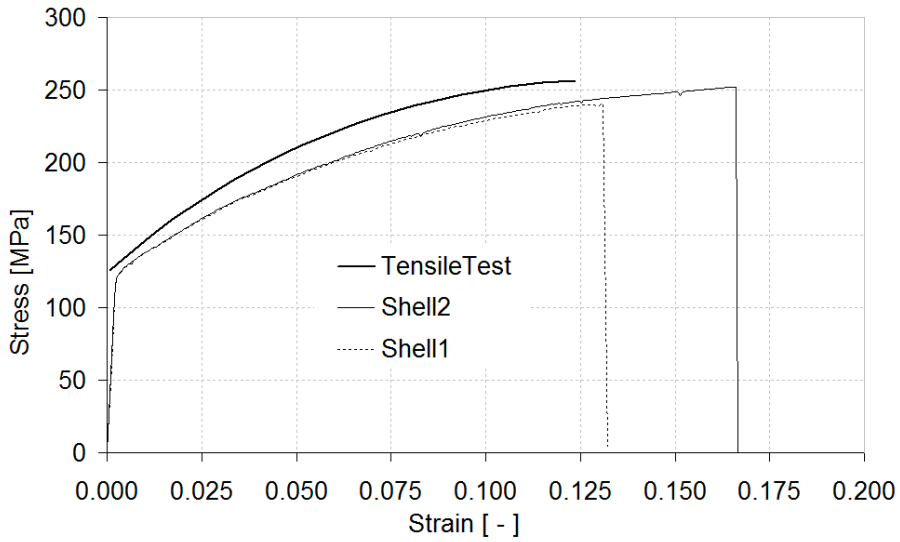

Figure 9 Numerical and experimental engineering stress–strain curves. Thickness 2.00 mm.

It is worth noting that the numerical simulations all predicted a fracture perpendicular to the specimen axis, whereas in the thin tests, this fracture was inclined (Figure 7). This is due to the fact that the fracture process occurs at a molecular scale well below that of the mesh size and may be due to adjacent layers of atoms sliding over each other, resulting in a shear failure.

4. Numerical results and comparison with experimental tests

Firstly, various numerical models using the different mesh sizes and element type referred to in Section 3 were evaluated in terms of ability to predict the experimental results. In order to do this, a 'high' and a 'low' experimental impact velocity for each plate thickness were selected (represented in bold font in Table 1), and in each case the force-displacement responses numerically simulated and then compared with the corresponding experimental responses (Figures 10 – 13). Then, this information was used to select the 'best' models, which were then applied to calculate the maximum force and displacement values for the whole range of experimental impact velocities considered here.

For the thick plates, Figures 10 and 11 show that, for both velocities, the Shell2 model approximates the experimental plastic response well and that the coarser meshed Shell4 and Shell6 are less accurate. For the solid element models, very similar results were obtained using both mesh sizes, but in terms of force-displacement prediction, they do not give better predictions than the computationally less demanding Shell2 model. Again, for both impact velocities, the deflection at which this maximum force is reached is generally underestimated by the numerical models; consequently, the maximum force is overestimated. Of the shell models, the Shell2 mesh gives the best prediction of this point, with both solid element models giving slightly better and very similar behaviour in this respect.

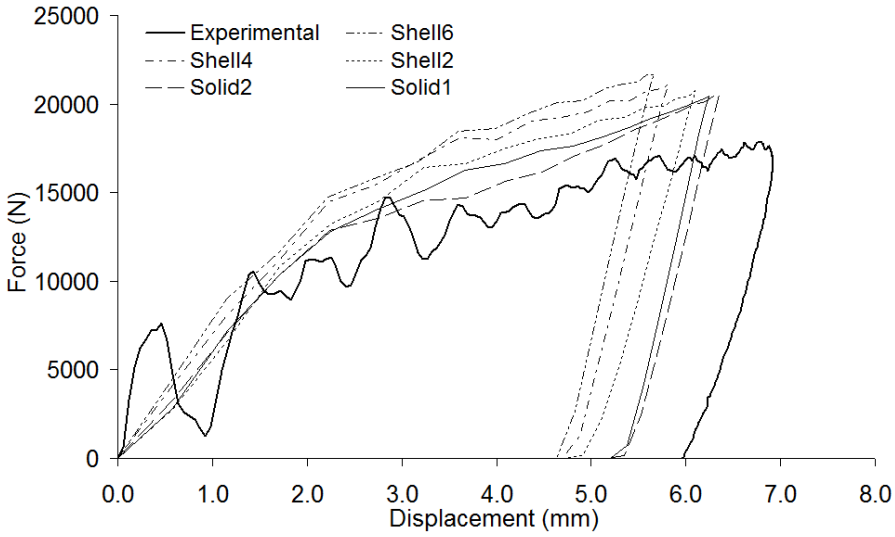

Figure 10 Force-displacement curves. Thick (5.92 mm) circular plates, impact velocity 5.85 m/s.

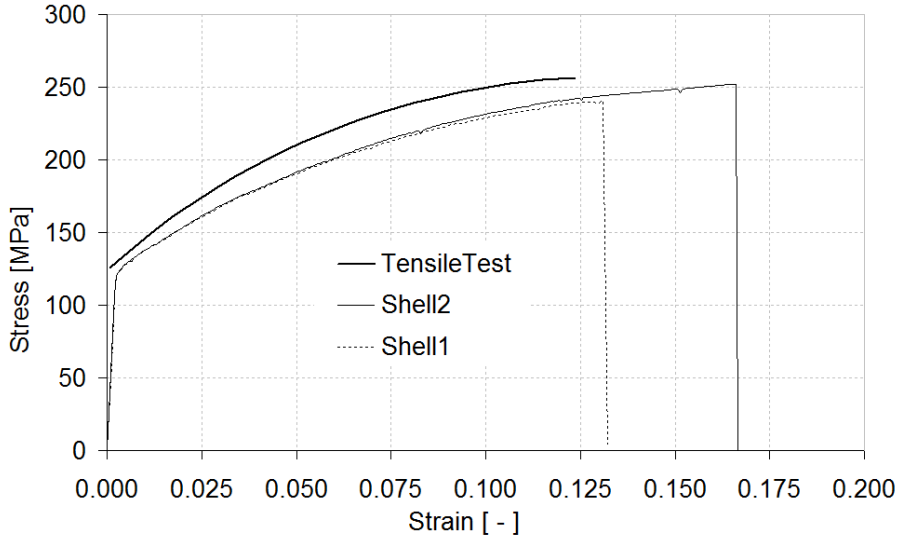

Figure 11 Force-displacement curves. Thick (5.92 mm) circular plates, impact velocity 2.62 m/s.

The oscillations seen in the responses could be due to the inertia of the plate and the contact stiffness (at the initiation of contact the impact mass and plate vibrate around the contact stiffness as the plate begins to move), or due to vibrations within the impact machine (most probably in the impact mass, which is in reality a hemispherical ended cylinder connected to a larger mass via a load cell). The contact-plate inertia oscillations would be apparent in both experimental and numerical responses, but vibrations in the test machine would only be apparent in the experimental response, since the impact mass is numerically modelled as a simple sphere. The fact that vibrations of the same frequency were noted in the experimental force measurements after separation of the impact mass and plate at the end of the impact event suggest that vibrations in the test machine were present in the experimental results. Since only contact-plate inertia oscillations are valid material impact responses, it would be pertinent to filter out any experimental oscillations

due to machine vibrations. However, in practice this filtering may well affect the impact response we wish to see, and it is extremely difficult to ensure that only the machine vibrations are filtered out. This shows that the filtering and interpretation of experimental impact test results is by no means a straightforward, clear-cut process, and further work is planned to clarify the exact nature of the oscillations seen. However, since the oscillations are harmonic and sufficient cycles occur prior to the end of the test, the energy values will be sufficiently accurate, and only the interpretation of the maximum load data could be open to discussion.

Prediction of the impact response is not the only criterion; it is also beneficial to predict well the shape of deformation due to both local indentation and global deflection. Here, it is relevant to remember that local 'indentation' can be thought of as consisting of (i) local out of plane plate deformations (where the plate 'wraps around' the indenter) and also (ii) the actual indentation of the indenter into the thickness of the plate material.

Figure 14 a shows that in this respect the Solid1 mesh gives a better definition of the shape of the deformation than does the Shell2 model. This is both because the finer mesh of the former is able to more accurately model the deformation around the indenter (cf. (i) above), and because a solid element is able to model the change in thickness of the material due to the indentation (cf. (ii) above).

Now, considering the thin plates, Figures 12 and 13 show that all of the shell mesh sizes considered give a good representation of the plastic force-displacement behaviour, especially at the higher impact velocity, and that the responses obtained from each of them are very similar. The use of more computationally expensive solid elements gives a very good fit to the experimental data even at the low impact velocity, where the shell models overestimate the force slightly.

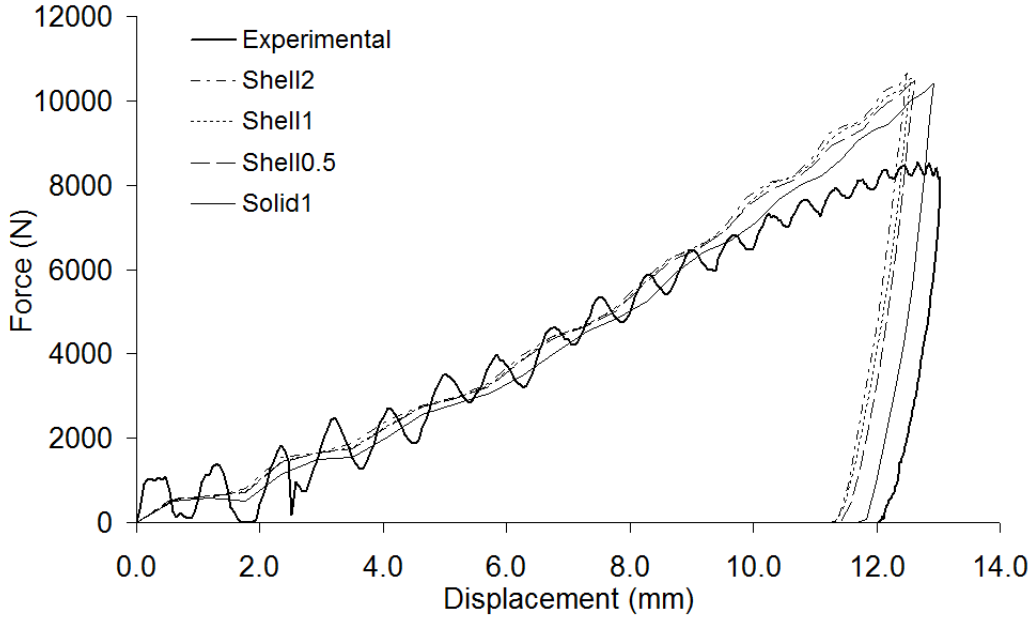

Figure 12 Force-displacement curves. Thin (2.00 mm) circular plates, impact velocity 5.90 m/s.

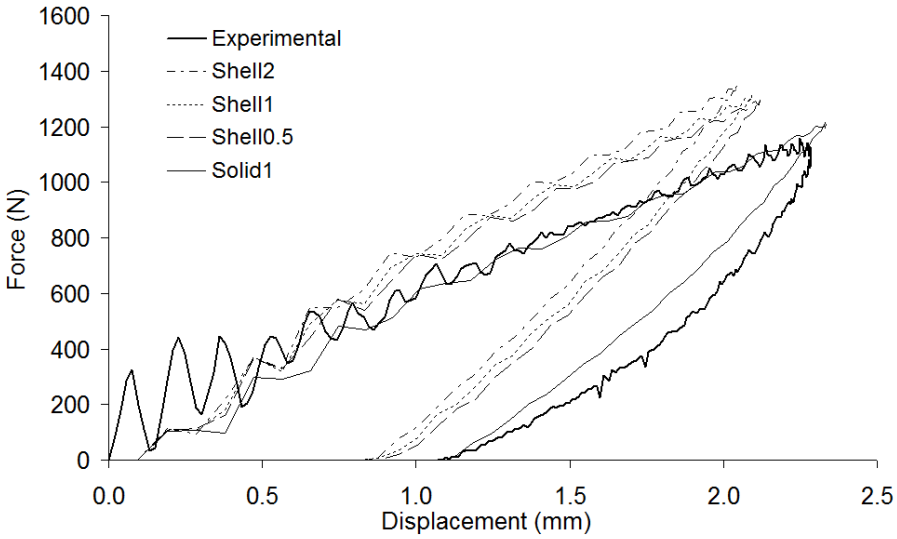

Figure 13 Force-displacement curves. Thin (2.00 mm) circular plates, impact velocity 0.95 m/s.

For the thin plates, indentation is more significant in terms of out of plane plate deformation but less significant in terms of indentation into the material thickness (Figure 14 b). Hence, here the only requirement is a fine mesh to adequately model the local deformation, with shell or solid elements giving similar representations.

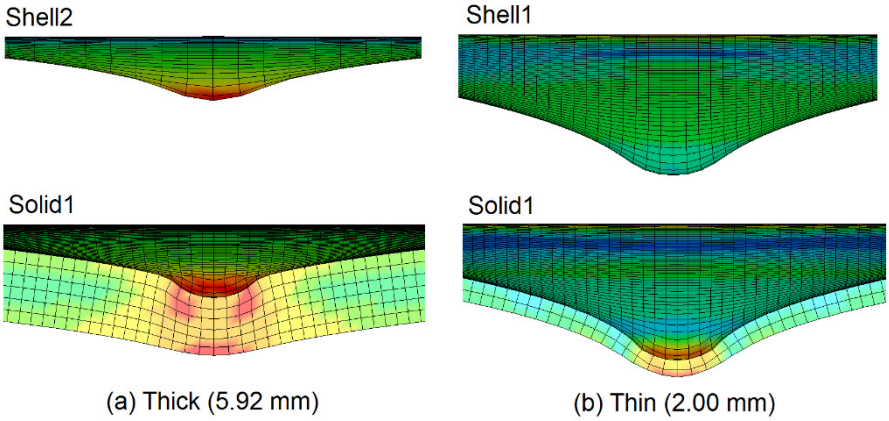

Figure 14 Shape of the deformation. (a) Thick (5.92 mm) circular plates, impact velocity 5.85 m/s. (b) Thin (2.0 mm) circular plates, impact velocity 5.90 m/s.

It should be noted at this point that though the experimental force-displacement curve is not always perfectly predicted by the numerical model, the time dependent curves of displacement and absorbed energy fit the experimental data very well.

The next step was to use the 'best' shell and solid models to simulate the remaining experimental impact velocities considered. As can be seen from Figures 15 to 18, the models predict the maximum deflection and maximum force very well. It is also apparent that, *when considering maximum force and deflection values only*, there is little if any significant differences between the various models and hence little advantage in using a more computationally-expensive element model.

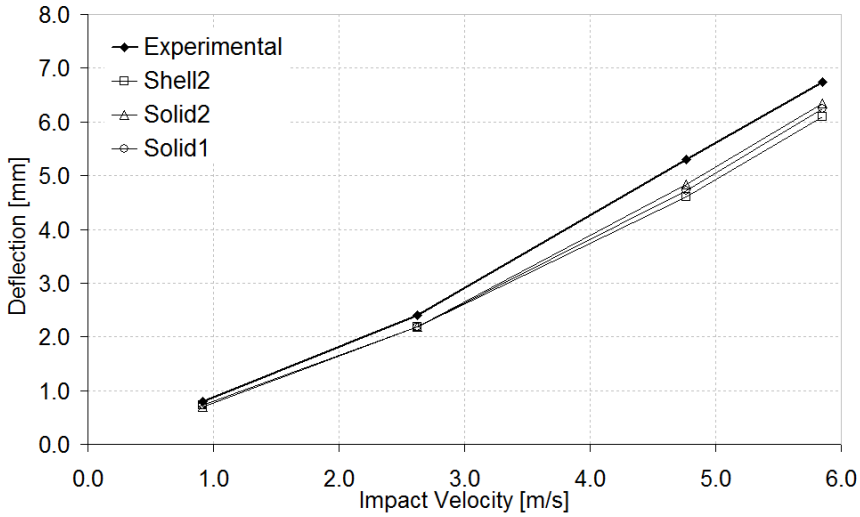

Figure 15 Maximum deflection versus impact velocity. Thick (5.92 mm) circular plates.

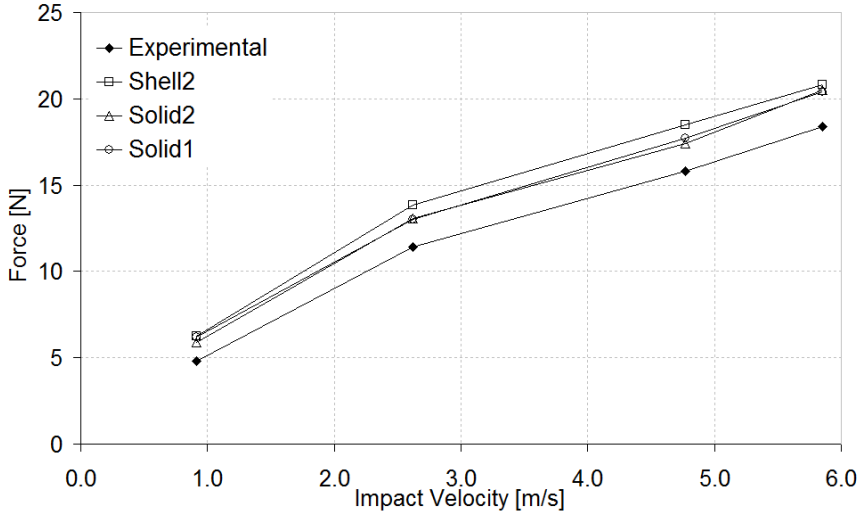

Figure 16 Maximum force versus impact velocity. Thick (5.92 mm) circular plates.

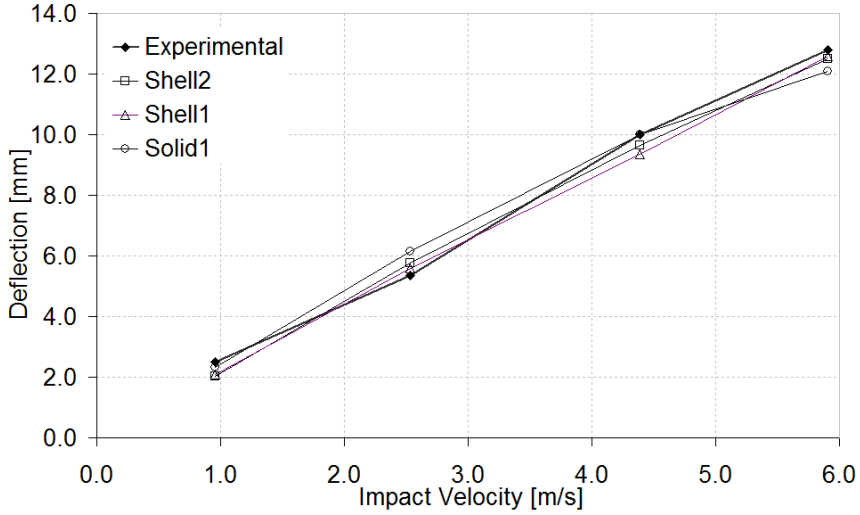

Figure 17 Maximum deflection versus impact velocity. Thin (2.00 mm) circular plates.

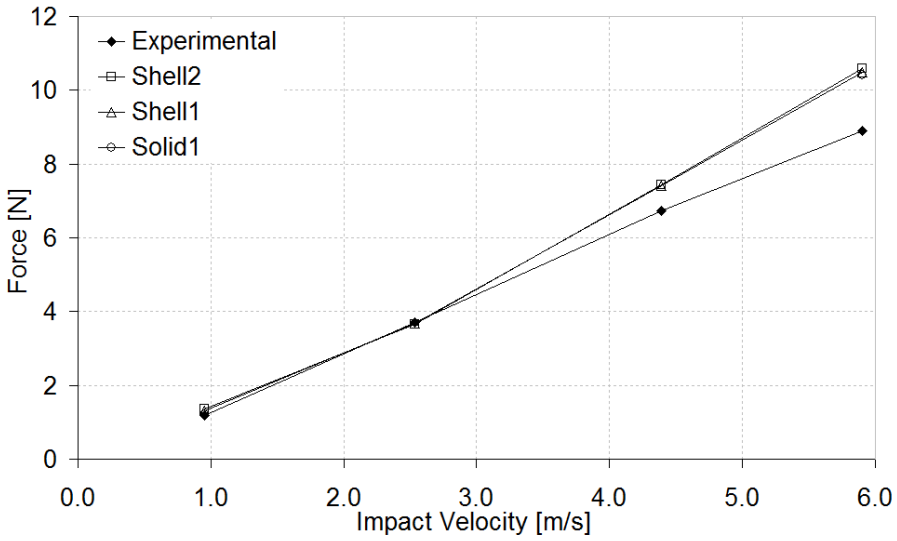

Figure 18 Maximum force versus impact velocity. Thin (2.00 mm) circular plates.

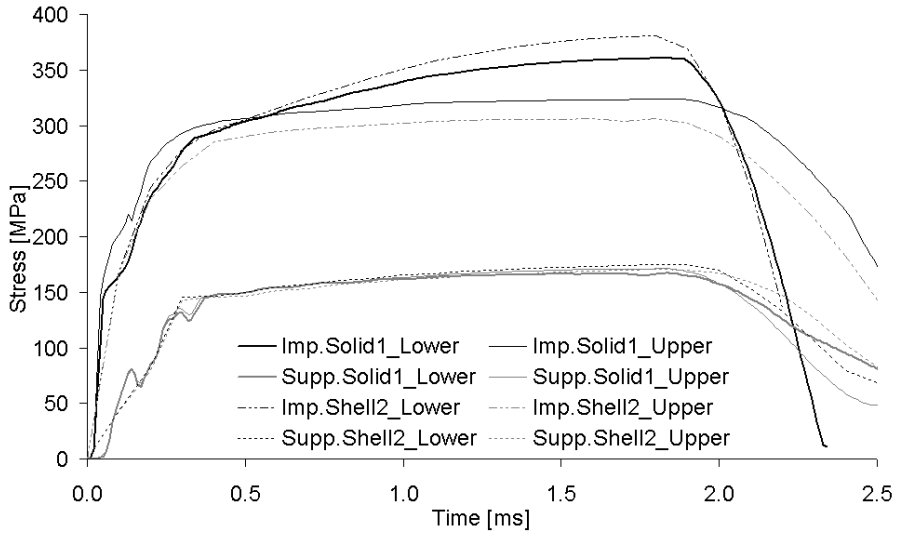

Figure 19 Effective stress with time. Thick (5.92 mm) circular plates, impact velocity 5.85 m/s.

The models showed that the maximum effective stress occurred on the lower surface opposite the impact point on both models shell and solid. The time variation of the effective stress is shown in Figure 19 for the thick circular plate with an incident velocity of 5.85 m/s as an example. Stress is shown for elements on the upper and lower surface at both the impact point and a point near the support. It can be seen from this figure that the maximum stress occurs on the surface opposite to the impact point, but that near the support, the stresses are almost the same on both sides of the plate. The maximum effective stress distribution in the solid model is also plotted in Figure 20 for the same impact event.

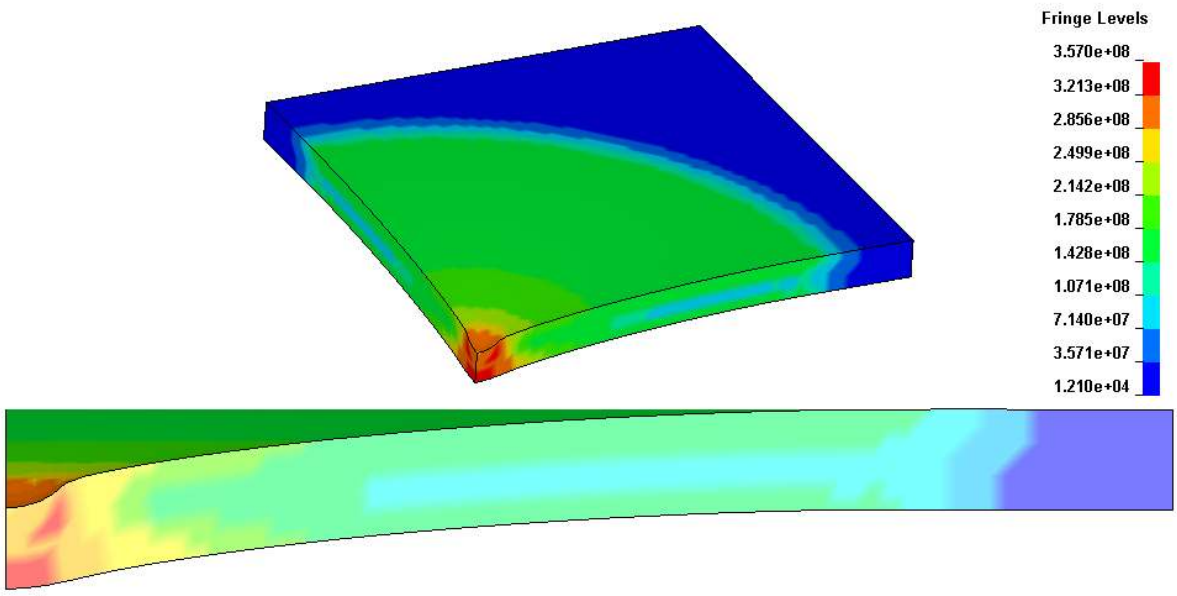

Figure 20 Maximum effective stress distribution. Thick (5.92 mm) circular plates, impact velocity 5.85 m/s.

The mass kinetic energy is dissipated as a combination of internal and sliding energies. For example, these values are plotted for the thick plate impacted at 2.62 m/s in Figure 21, where the magnitude of the sliding energy is about 13% of the dissipated kinetic energy using the Shell2 model, but only approximately 5% when the solid models are used. This implies that there is a small relative motion between the surface of the shell elements and the impacting mass, which is becoming less significant when solid elements are used. This could be because the indentation into the material thickness is modelled only in the case of solid elements, hence resisting sliding. This may require further investigation.

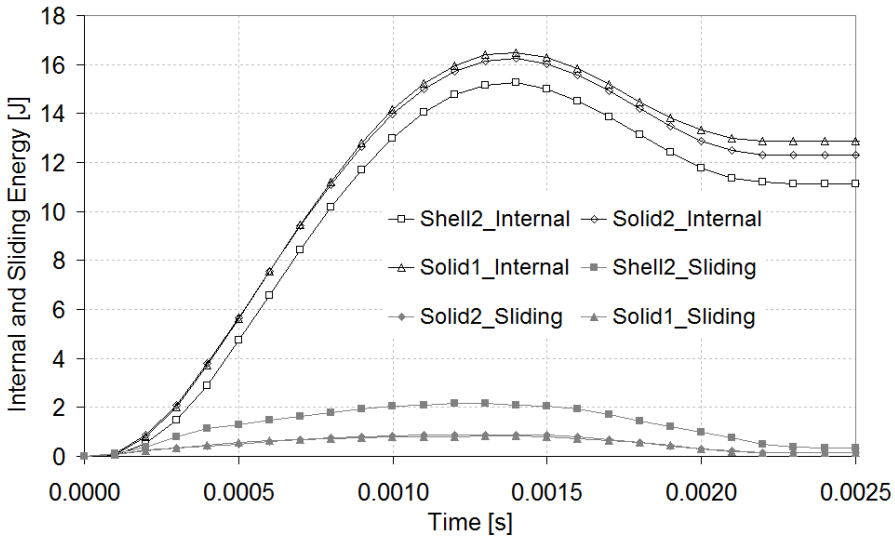

Figure 21 Internal and sliding energy dissipation. Thick (5.92 mm) circular plates, impact velocity 2.61 m/s.

Overall, good agreement between numerical and experimental results was obtained, especially for the thin plates; for the thick plates, some discrepancies between theory and test results were noted, the possible reasons for which are discussed below.

It is possible that the actual experimental clamped condition was not as perfect as represented in the numerical model; it is quite possible that some slippage between the support plates was experienced by the specimen plate, and in fact all of the tested plates experienced greater displacements than predicted by the FE models. The numerical clamped condition is affected by the static coefficient of friction in the contact definition between support and specimen plates; for example, decreasing this coefficient gives greater displacements and lower forces, giving a better approximation between experimental and numerical results. Further work would be beneficial to further refine the model in terms of this coefficient.

The true stress–strain curve material definition input to the numerical model is also a possible source for discrepancies; here, these values were obtained using tensile test specimens cut from the same plates from which the impact specimens were taken, and the data differed from that supplied by the plate manufactures. Another possible material property source of errors is the strain-rate effect, which was not considered in the current numerical model. A search of the literature showed that Cowper–Symonds data for aluminium 5083/H111 is not available, and since these coefficients have been seen to vary greatly between specific aluminium alloys, values for other alloys could not be used. Preliminary studies into the effect of strain rate have shown that further work to obtain this data could improve the accuracy of the maximum displacement results calculated here.

In this study, some of the parameters that affect the impact response were varied to optimise the FE model (e.g. mesh size and element type), but others were set at constant values obtained from the literature or not included (e.g. static coefficient of friction and strain-rate parameters) in order to keep the size of the investigation practicable. However, further work could now investigate the effects of all of the parameters, especially if labour-saving techniques such as those of statistical experimental design (Sutherland and Guedes Soares 2003) were used to ensure a practical number of modelling runs and, importantly, to ensure that any interactions between these parameters are correctly identified.

Finally, as mentioned in the introduction, in analysing the structural response of ship collisions it is necessary to analyse first individually the structural members under lateral impact loads. It is well known that the structural design of ships is achieved using mainly plating, longitudinal stiffeners and frames. In a collision the plates of the ship suffer the most severe consequences, and the permanent deformations are generally greater than the plate thickness and may extend across more than the frame spacing. Thus this analysis will be used as a base for further FE analyses of stiffened plates subjected to large deformation under lateral impact.

5. Conclusions

Detailed information of the impact response of clamped aluminium 5083 circular plates has been obtained through non-linear explicit dynamic simulation using the LS-DYNA software package. The results obtained were in good agreement with experimental tests, indicating that even computationally inexpensive coarse meshes using shell elements are sufficient to

predict the maximum deflections and forces. However, finer meshed shell and solid element models give better prediction of the force-displacement behaviour. Where small discrepancies between numerical and experimental results occurred, this was due to overestimation of the impact force, whereas the variation of displacement with time was generally very well predicted.

The numerical simulations give a good understanding of the shape of the deformation in plates subjected to impact loading, and a fine meshed solid model is needed to give a good approximation of the deformation shape, especially where local indentation is significant. In the present work, the study of the effect of mesh size showed that the ratio of element size to indenter radius should preferably be approximately 1/5 in order to satisfactorily define the shape of the deformation.

The material true stress–strain curve inputs to the numerical model were obtained from tensile tests on the actual material used to fabricate the impacted plates. This was simplified since the test maximum load was almost coincident with the rupture load, but for other materials, it may be more difficult to define the true stress–strain curve and approximations such as the power law curve must be included.

The numerical models were successfully used to predict the impact response of aluminium 5083 plates, and the next planned stage of this work is to see if the technique is also successful for steel plate impact tests. For example, strain rate does not seem to play an important role in numerical simulation of these aluminium plates; however, this may not be the case for other materials.

Acknowledgments

[Acknowledgements] The work has been performed in the scope of the project MARSTRUCT, Network of Excellence on Marine Structures (http://www.mar.ist.utl.pt/marstruct/), which has been financed by the European Union through the GROWTH Programme under contract TNE3-CT-2003-506141.

The first author has been financed by the Portuguese Foundation for Science and Technology (Fundação para a Ciência e Tecnologia), under contract SFRH/BD/46369/2008.

References

Akita Y, Ando N, Fujita Y, Kitamura K. 1972. Studies on collision-protective structures in nuclear powered ships. Nucl Engng Des. 19: 365 - 401.

Amdahl J, Kavlie D, Johansen A. 1995. Tanker grounding resistance. Proc. 6th Int. Symp. on Practical Design of Ships and Mobile Units (PRADS'95). 1072 - 1083.

Dieter GE. 1986. Mechanical behavior under tensile and compressive loads. ASM Handbook. 8: 99-10.

Ehlers S. 2010. Strain and stress relation relation until fracture for finite element simulations of a thin circular plate. Thin-Walled Structures. 48 (1): 1 - 8.

Ehlers S, Varsta P. 2009. Strain and stress relation for non-linear finite element simulations. Thin-Walled Structures. 47 (11): 1203 - 1217.

Ehlers S, Klanac A, Tabri K. 2007. Increased safety of a tanker and ropax vessel by implementing a novel sandwich structure. 4th International Conference on Collision and Grounding of Ships: Hamburg, Germany. 109 - 115.

Guedes Soares C. 1981. A Mode solution for the finite deflections of a circular plate loaded impulsively. Engineering Transactions. 29 (1): 99 - 114.

Hallquist JO. 2005. LS-DYNA Theory Manual. Livermore Software Technology Corporation.

Jones N. 1989. Structural Impact. Cambridge University Press.

Kajaste-Rudnitski J, Vastra P, Matusiak J. 2005. Some finite element estimates of ship collision event. Maritime Transportation and Exploitation of Ocean and Coastal Resources, Guedes Soares, Garbatov & Fonseca (eds).Taylor & Francis Group, London. 447 - 453

Liu J, Jones N. 1987. Experimental investigation of clamped beams struck transversely by a mass. International Journal of Impact Engineering. 6 (4): 305 - 335.

McDermott JF et al. 1974. Tanker structural analysis for minor collision. Trans SNAME. 82: 382 - 407.

Shen WQ. 1995. Dynamic plastic response of thin circular plates struck transversely by nonblunt masses. Int. J. Solids Structures. 32 (14): 2009 - 2021.

Shen W.Q. 2002. A study on the failure of circular plates struck by masses. Part 2: theoretical analysis for the onset of failure. International Journal of Impact Engineering 27 (4): 413 - 432.

Shen WQ, Rieve NO, Baharun B. 2002. A study on the failure of circular plates struck by masses. Part 1: experimental results. International Journal of Impact Engineering. 27 (4): 399 - 412.

Simonsen BC, Lauridsen LP. 2000. Energy absorption and ductile failure in metal sheets under lateral indentation by a sphere. International Journal of Impact Engineering. 24 (10): 1017 - 1039.

Stronge WJ, Yu TX. 1993. Dynamic Models for Structural Plasticity. © Springer-Verlag London Limited.

Sutherland LS, Guedes Soares C. 2003. The effects of test parameters on the impact response of glass reinforced plastic using an experimental design approach. Composites Science and Technology. 63: 1 - 18.

Sutherland LS, Guedes Soares C. 2009. Impact behaviour of GRP, aluminium and steel plates. Analysis and Design of Marine Structures; Guedes Soares & Das (eds). Taylor & Francis Group: London. 293 – 300

Tabri K, Alsos H, Broekhuijsen J, Ehlers S. 2007. A benchmark study on ductile failure criteria for shell elements in multiaxial stress state. Advancements in Marine Structures, Guedes Soares & Das (eds). Taylor & Francis Group: London. 401-409.

Wang G, Ohtsubo H, Arita K. 1998. Large deflection of a rigid-plastic circular plate pressed by a sphere. Journal of Applied Mechanics. 65 (2): 533 - 535.

Wang G, Ohtsubo H, Liu D. 1997. A simple method for predicting the grounding strength of ships. J Ship Res. 41: 241 - 247.

Yu TX, Chen FL. 2000. Failure of plastic structures under intensive dynamic loading: Modes, criteria and thresholds. Int. J. of Mechanical Science. 42: 1531 - 1554.